Context-Dependent Development of Lymphoid Stroma from Adult CD34+ Adventitial Progenitors

Sitnik, Katarzyna Maria; Wendland, Kerstin; Weishaupt, Holger; Uronen-Hansson, Heli; White, Andrea J.; Anderson, Graham; Kotarsky, Knut; Agace, William Winston

Published in:
Cell Reports

Link to article, DOI:
10.1016/j.celrep.2016.02.033

Publication date:
2016

Document Version
Publisher's PDF, also known as Version of record

Article

Cell Reports

Context-Dependent Development of Lymphoid Stroma from Adult CD34+ Adventitial Progenitors

Graphical Abstract

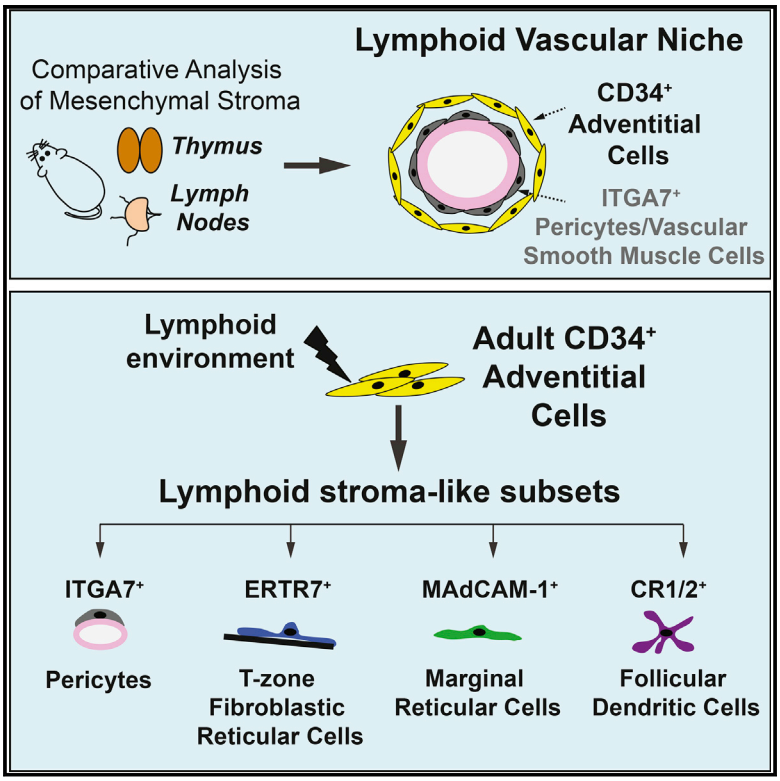

Highlights

- CD34+ stromal cells localize to the adventitial vascular niche in lymphoid tissues
- Thymic CD34+ cells and pericytes derive from a common anlage-seeding population
- Adult CD34+ adventitial cells have lymphoid stroma-like progenitor potential
- Lymphoid environment regulates the differentiation of CD34+ adventitial progenitors

Authors

Katarzyna M. Sitnik, Kerstin Wendland, Holger Weishaupt, ..., Graham Anderson, Knut Kotarsky, William W. Agace

Correspondence

kasit@vet.dtu.dk (K.M.S.), william.agace@med.lu.se (W.W.A.)

In Brief

Sitnik et al. comparatively assess the stromal cell composition of the thymus and lymph nodes. The authors identify CD34+ adventitial cells as a conserved component of the thymic and lymph node vascular niche and demonstrate that this subset contains adult progenitors with lymphoid stroma-like subset potential in vivo.

Accession Numbers

GSE76974

Sitnik et al., 2016, Cell Reports *14*, 2375–2388
March 15, 2016
http://dx.doi.org/10.1016/j.celrep.2016.02.033

CellPress

Cell Reports
Article

Context-Dependent Development of Lymphoid Stroma from Adult CD34$^+$ Adventitial Progenitors

Katarzyna M. Sitnik,[1,*] Kerstin Wendland,[2] Holger Weishaupt,[3] Heli Uronen-Hansson,[2] Andrea J. White,[4] Graham Anderson,[4] Knut Kotarsky,[2] and William W. Agace[1,2,*]
[1]Section for Immunology and Vaccinology, National Veterinary Institute, Technical University of Denmark, Bülowsvej 27, 1870 Frederiksberg C, Denmark
[2]Immunology Section, Lund University, BMC D14, 221-84 Lund, Sweden
[3]Department of Immunology, Genetics, and Pathology, Rudbecklaboratoriet, Uppsala University, 751-85 Uppsala, Sweden
[4]Medical Research Council Centre for Immune Regulation, Institute for Biomedical Research, University of Birmingham, Birmingham B15 2TT, UK
*Correspondence: kasit@vet.dtu.dk (K.M.S.), william.agace@med.lu.se (W.W.A.)
http://dx.doi.org/10.1016/j.celrep.2016.02.033

SUMMARY

Despite the key role of primary and secondary lymphoid organ stroma in immunity, our understanding of the heterogeneity and ontogeny of these cells remains limited. Here, we identify a functionally distinct subset of BP3$^-$PDPN$^+$PDGFRβ$^+$/α$^+$CD34$^+$ stromal adventitial cells in both lymph nodes (LNs) and thymus that is located within the vascular niche surrounding PDPN$^-$PDGFRβ$^+$/α$^-$Esam-1$^+$ITGA7$^+$ pericytes. CD34$^+$ adventitial cells developed in late embryonic thymus and in postnatal LNs and in the thymus originated, along with pericytes, from a common anlage-seeding progenitor population. Using lymphoid organ re-aggregate grafts, we demonstrate that adult CD34$^+$ adventitial cells are capable of differentiating into multiple lymphoid stroma-like subsets including pericyte-, FRC-, MRC-, and FDC-like cells, the development of which was lymphoid environment-dependent. These findings extend the current understanding of lymphoid mesenchymal cell heterogeneity and highlight a role of the CD34$^+$ adventitia as a potential ubiquitous source of lymphoid stromal precursors in postnatal tissues.

INTRODUCTION

Lymphoid organs, such as the thymus and lymph nodes (LNs), play essential roles in the development and functionality of the adaptive immune system. Accordingly, the thymus is the major site of T cell development while LNs support naive T and B cell survival, facilitate their encounter of antigens, and aid in the regulation of effector T and B cell responses. While these functions critically depend on the activity of specialized stromal cell populations, including cells of mesenchymal origin, our understanding of mesenchymal subset specialization and ontogeny in lymphoid tissues remains limited. In LNs, CD45$^-$CD31$^-$ LN mesenchymal cells (LNMC) are classically distinguished into podoplanin$^+$ (PDPN$^+$) and PDPN$^-$ subsets. Approximately 60%–70% of PDPN$^-$ LNMC express the integrin α7β1 and include contractile pericytes (Malhotra et al., 2012) while PDPN$^+$ LNMC are distinguished into three distinct subsets; fibroblastic reticular cells (FRC), follicular dendritic cells (FDC), and marginal reticular cells (MRC). FRC wrap around the reticular network of ERTR7$^+$ collagen-rich fibers in the LN paracortex and contain cells expressing CCR7 ligands (CCL19 and CCL21), IL-7, cholesterol 25-hydroxylase, and B cell activating factor (BAFF) and have been implicated in supporting the homing/migration/survival of T cells (Chang and Turley, 2015; Girard et al., 2012; Link et al., 2007; Yi et al., 2012). In contrast to FRC, FDC and MRC express high protein levels of CXCL13 (Katakai et al., 2008). FDC represent a B cell follicle-resident population, selectively expressing complement receptor CR-1 (CD35) and CR-2 (CD21), that support B cell follicular organization and germinal center reactions (Wang et al., 2011) while MRC are characterized as a population of mucosal vascular addressin cell adhesion molecule-1 (MAdCAM-1) and receptor activator of nuclear factor kappa-B ligand (RANKL) expressing cells of unclear immunological function located underneath the LN subcapsular sinus (Katakai et al., 2008).

Similar to LNMC, thymic mesenchymal cells (TMC) have been implicated in a range of immunological processes including support of early thymus organogenesis (Gordon and Manley, 2011), regulation of thymic epithelial cell (TEC) homeostasis (Jenkinson et al., 2007; Sitnik et al., 2012), and thymocyte egress (Zachariah and Cyster, 2010). TMC are located in the capsule and surrounding the vasculature of both thymic cortical and medullary regions, with some displaying pericyte morphology in situ (Müller et al., 2008). Several phenotypic markers have been utilized to identify and/or isolate TMC, including platelet-derived growth factor receptor α (PDGFRα) and platelet-derived growth factor receptor β (PDGFRβ) (Gray et al., 2007; Odaka, 2009), PDPN (Sitnik et al., 2012), and Ly51 (Müller et al., 2008), however, whether the TMC compartment consists of functionally distinct subsets as well as the functional and developmental relationship between TMC and LNMC subsets remain unknown.

While our knowledge of LNMC and TMC heterogeneity remains limited, even less is known regarding the ontogenic development of these cells. During thymus organogenesis, PDGFRα$^+$

mesenchymal cells form an organ capsule around the thymic epithelial anlagen as it detaches from the third pharyngeal pouch endoderm at E12.5 (Gordon and Manley, 2011) followed by migration inside the epithelial core by E13.5 (Mori et al., 2010). Similarly, during inguinal LN development, PDGFRα$^+$ mesenchyme encircles a bulged outgrowth of newly specified lymphatic endothelium called a lymph sac at E14.5 and subsequently infiltrates the endothelial core by E17.5 (Bénézech et al., 2010). Whether all mature TMC and LNMC subsets can be derived from a common population of anlage-seeding progenitors and the phenotype of such putative precursor remain unclear.

In the present study, through comparative analysis of LN and thymic stroma, we identify CD34$^+$ adventitial cells as a conserved component of the postnatal thymic and lymph node vascular niche and demonstrate at the population level that these cells contain progenitors capable of generating FRC-, MRC-, and FDC-like cells as well as pericytes. In addition, we provide data to suggest that lymphoid CD34$^+$ adventitial cells develop, along with other lymphoid mesenchymal subsets, from BP-3$^-$PDPN$^+$PDGFRβ$^+$/α$^+$CD34$^{-/lo}$Esam-1$^-$ anlage-seeding mesenchymal precursors.

RESULTS

Phenotypic and Global Gene Expression Profiling Identifies Similar and Distinct Stromal Subsets between the Thymus and LNs

To gain a better understanding of the heterogeneity and function of mesenchymal stromal cells in lymphoid organs, we compared mesenchymal cell subset composition in digested thymic and pooled inguinal, brachial, and axillary LNs from 6- to 9-week-old mice by flow cytometry. In both the thymus and LNs, a major fraction of CD45$^-$EpCAM$^-$CD31$^-$ cells expressed the mesenchymal cell marker, PDGFRβ (hereafter referred to as thymic and LN mesenchymal cells [TMC and LNMC], respectively) together with a variably detectable population of CD45$^-$EpCAM$^-$CD31$^-$PDGFRβ$^-$ cells (Figure 1A). Distinct PDPN$^+$PDGFRα$^+$ and PDPN$^-$PDGFRα$^-$ITGA7$^+$ mesenchymal subsets have previously been identified in LNs (Malhotra et al., 2012), and we have recently shown that thymic mesenchymal cells comprise PDPN$^+$Ly51^{int} and PDPN$^-$Ly51^{hi} populations (Sitnik et al., 2012). Comparative phenotypic analysis revealed that both LNMC and TMC were composed of a dominant population of PDPN$^+$PDGFRα$^+$Ly51^{int} and a minor population of PDPN$^-$PDGFRα$^-$ITGA7$^+$Ly51^{hi} cells (Figure 1B). A substantial fraction of PDPN$^+$ LNMC, but not TMC, expressed bone marrow stromal cell antigen-1 (BP-3) (Figure 1B). Similar subset composition characterized the LNMC compartment in mesenteric LNs (data not shown). To assess the relationship between TMC and LNMC subsets, global gene expression analysis was performed on sorted PDPN$^-$ and BP-3$^-$PDPN$^+$ and BP-3$^+$PDPN$^+$ LNMC as well as PDPN$^-$ and PDPN$^+$ TMC (hereafter termed BP-3$^-$PDPN$^+$ TMC) from 2-week-old mice by microarray (for sorting strategy see Figures S1A and S1B). Such analysis confirmed differential expression at the mRNA level of the phenotypic markers used to define each population (Figure S1C). Matrix plots of population similarity measured by Pearson correlation coefficient confirmed reproducibility within the triplicate datasets (Figure S1D) and together with hierarchical clustering and PCA analysis demonstrated that PDPN$^-$ TMC most closely resembled PDPN$^-$ LNMC while BP-3$^-$PDPN$^+$ TMC most closely resembled BP-3$^-$PDPN$^+$ LNMC. BP-3$^+$PDPN$^+$ LNMC were more similar to BP-3$^-$PDPN$^+$ LNMC and TMC than to PDPN$^-$ LNMC and TMC (Figures 1C and 1D). Comparison of transcriptional profiles between PDPN$^-$ and BP-3$^-$PDPN$^+$ TMC and between PDPN$^-$ and BP-3$^-$PDPN$^+$ LNMC identified 1,760 and 1,498 differentially expressed genes (>2-fold change [FC]; p value [Benjamini-Hochberg, pBH] < 0.05; expressed in at least one of compared subsets) (data not shown). Notably, global changes in gene expression between PDPN$^-$ and BP-3$^-$PDPN$^+$ TMC correlated significantly with changes between PDPN$^-$ and BP-3$^-$PDPN$^+$ LNMC; >90% of probe sets that differed >2-fold between PDPN$^-$ TMC and BP-3$^-$PDPN$^+$ TMC were similarly up- or down-regulated between the corresponding subsets in the LNs (probe sets expressed in at least one TMC and LNMC subset; CV < 0.5 for all subsets) (Figure 1E).

PDPN$^-$ and BP-3$^-$PDPN$^+$ Cells Form Specialized Components of the Vascular Niche

Immunohistochemical analysis has previously indicated that LN FDC, MRC, and T-zone FRC express BP-3 (Katakai et al., 2008; Link et al., 2007). We thus determined whether such populations were present within BP-3$^+$PDPN$^+$ LNMC. A fraction of BP-3$^+$PDPN$^+$ LNMC, but not BP-3$^-$PDPN$^+$ LNMC or TMC, expressed intracellular CCL21 protein, and a subset of BP-3$^+$PDPN$^+$ LNMC expressed MAdCAM-1. BP-3$^+$PDPN$^+$ LNMC also demonstrated the highest mRNA levels of genes associated with FRC and MRC (Figures 2A, 2B, and S2A). Further, staining for the FDC markers, CR-1 (CD21) and CR-2 (CD35), demonstrated that CR1/2$^+$PDPN$^+$ FDC were BP-3$^+$ and PDGFRβ$^{-/lo}$ (Figure 2C). Collectively, these results demonstrate that BP-3$^+$PDPN$^+$ LNMC include CCL21$^+$ FRC, MRC, and FDC, and that these subsets are absent from steady-state thymus.

Gene sets associated with vascular smooth muscle cell (VSMC) contractility (Malhotra et al., 2012) and pericyte identity (Armulik et al., 2011) were highly expressed by PDPN$^-$ compared to PDPN$^+$ TMC and LNMC (Figure 2D), which correlated with the specific detection of high levels of α-smooth muscle actin, αSMA in a proportion of these cells (Figure 2E). Thus, PDPN$^-$ TMC and LNMC appear to contain both contractile and non-contractile pericytes. PDPN$^-$ TMC and the majority of PDPN$^-$ LNMC, but not PDPN$^+$, populations also expressed endothelial cell-selective adhesion molecule-1, Esam-1 (Figures 2D and 2F). Analysis of the remaining BP-3$^-$PDPN$^+$ LNMC and TMC subsets demonstrated that these cells expressed highest levels of CD34 (Figure 2G), a sialomucin expressed by mesenchymal adventitial cells in human arteries and veins (Corselli et al., 2012).

To assess the localization of BP-3$^-$PDPN$^+$CD34$^+$ and PDPN$^-$ LNMC and TMC, immunohistochemical staining was performed on thymic and LN sections. PDGFRβ$^+$/α$^-$ (PDPN$^-$) TMC were detected in direct association with CD31$^+$ vascular endothelium of capillaries (Figures S2B and S2C, arrowheads) as well as arterioles (data not shown) and venules within the thymic cortex, cortico-medullary junction (CMJ), and medulla (Figure 2H, arrowheads). In agreement with previously reported distribution

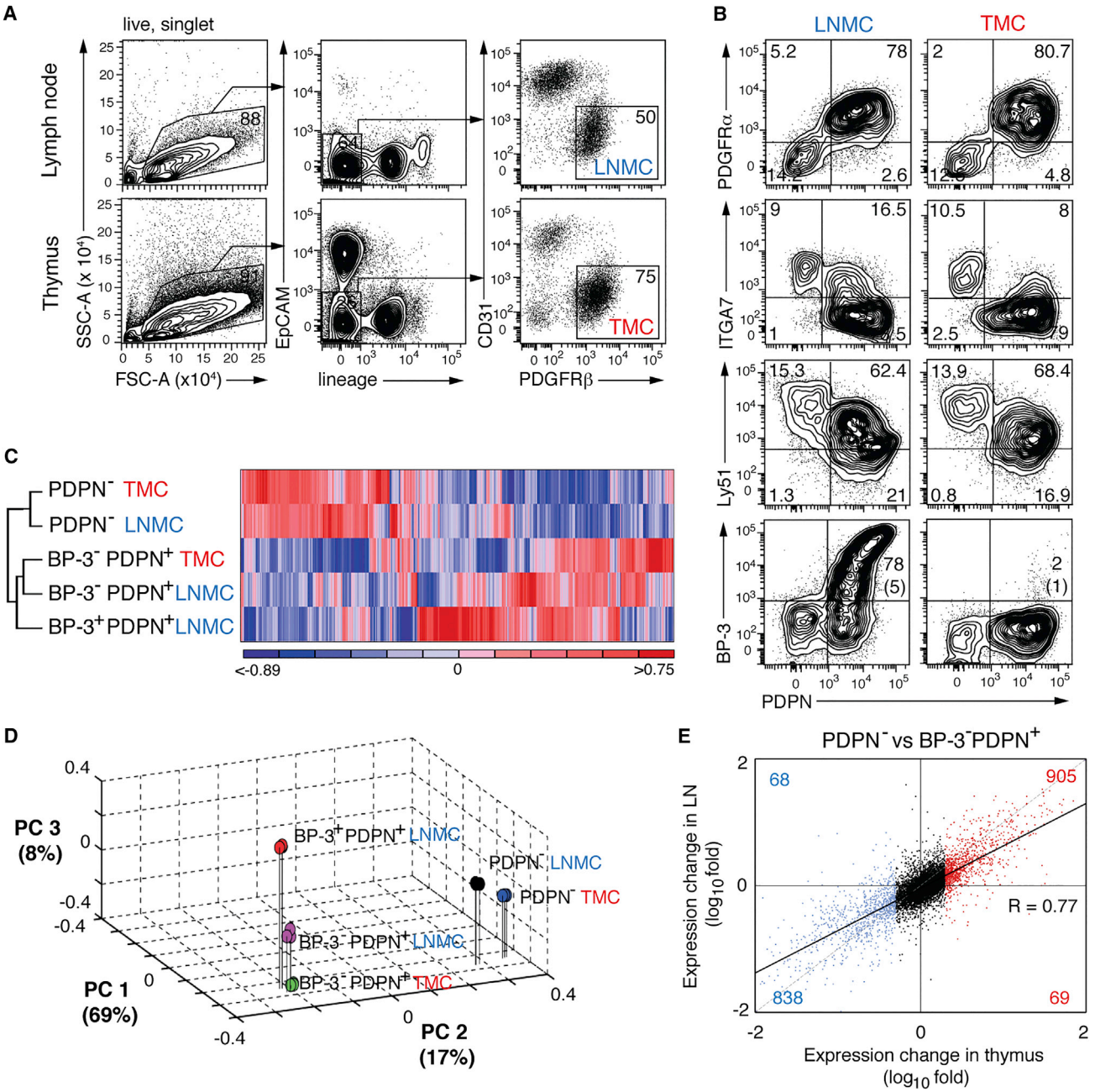

Figure 1. Comparison of Lymph Node and Thymic Mesenchymal Cell Subsets

(A and B) Identification (A) and phenotype (B) of PDGFRβ$^+$ mesenchymal cells from pooled inguinal, brachial, and axillary LNs (LNMC) and thymus (TMC) from 6- to 9-week-old mice. (A) Lineage; CD45, Ter119, CD11b, CD11c, NK1.1, Gr-1, B220. Numbers are percentage of cells within indicated gates or mean percentage (SD) within PDPN$^+$ cells (BP-3). (B) Data are from one representative experiment of three (PDGFRα, ITGA7, Ly51) or ten (BP-3) performed using pooled cells from one to six mice per experiment.

(C–E) Comparative gene expression analysis of LNMC and TMC subsets from 2-week-old mice. For sorting strategy see Figure S1. (C) Hierarchical clustering of the 4,523 genes with greatest changes in gene expression. (D) Principal component (PC) analysis. Numbers in brackets represent the percentage of total variability accounted for by each PC. (E) Scatter plot of the fold changes in gene expression between PDPN$^-$ and BP3$^-$PDPN$^+$ TMC (x axis) and LNMC (y axis). Each dot represents one probe set. Probe sets downregulated or upregulated >2-fold in PDPN$^-$ compared to BP3$^-$PDPN$^+$ TMC are shown in blue and red, respectively. The dashed gray line represents the diagonal and the black solid line depicts the regression line fitted through all data points. R value indicates the Pearson correlation coefficient between the two datasets. Numbers indicate the total number of probes of that color within indicated quadrants.

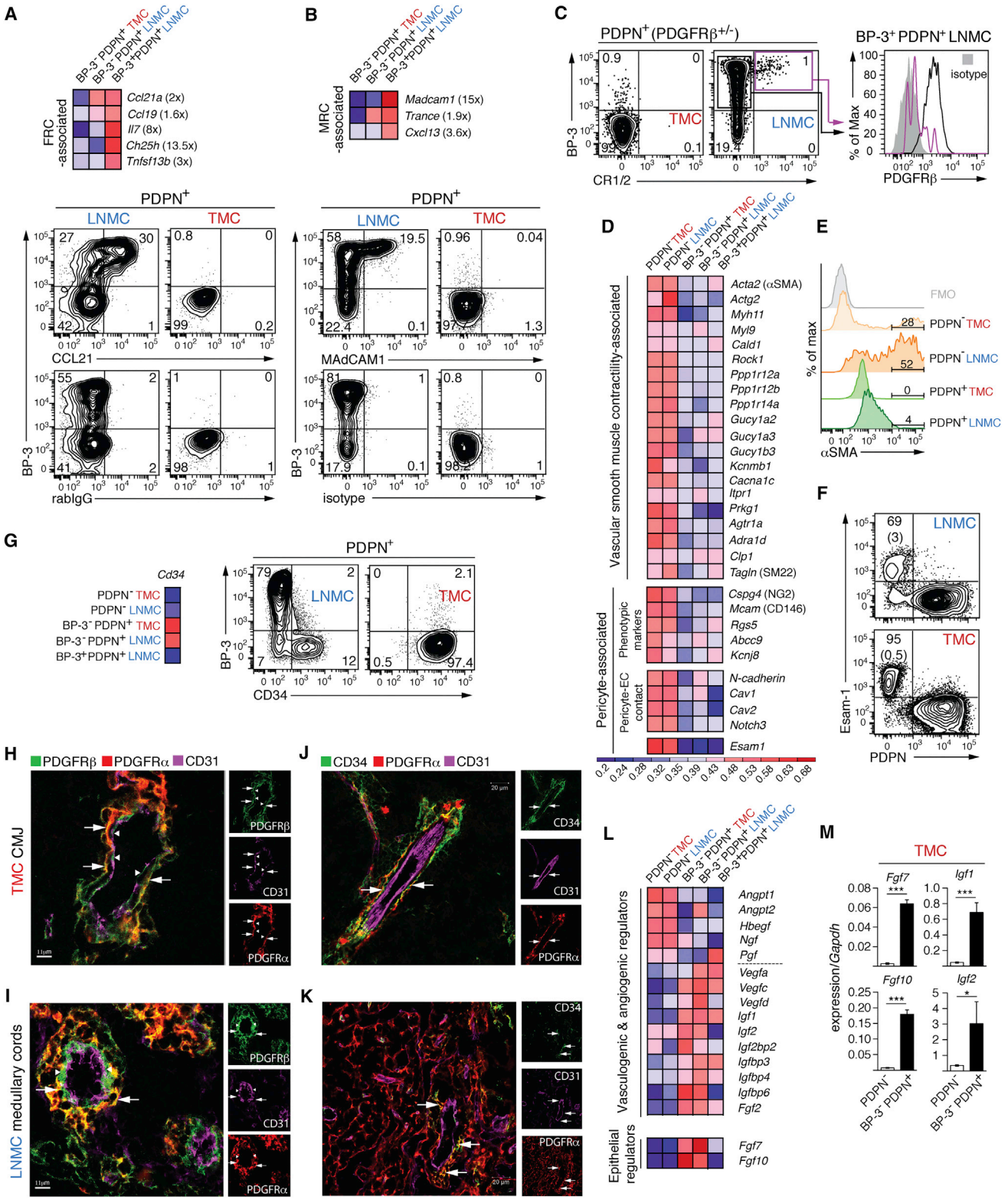

Figure 2. PDPN⁻ and BP3⁻PDPN⁺ TMC and LNMC Represent Specialized Components of the Vascular Niche

(A–G, L) Heatmaps of expression values of selected genes expressed by LNMC and TMC subsets. Data are log2 transformed and row normalized. Numbers in brackets are fold difference in the expression of the indicated genes between BP3⁺PDPN⁺ and BP3⁻PDPN⁺ LNMC. (A and B) PDGFRβ⁺PDPN⁺ or (C)

(legend continued on next page)

of ITGA7$^+$ LNMC (Malhotra et al., 2012), PDGFRβ$^+$/α$^-$ (PDPN$^-$) LNMC were found in direct contact with the CD31$^+$ endothelium of cortical and medullary vessels as well as lining the lymphatic endothelium of the subcapsular sinus (Figure 2I; data not shown). Thus, the distribution of PDGFRβ$^+$/α$^-$ (PDPN$^-$) TMC and LNMC fitted with their transcriptional identification as pericytes. In contrast, CD34 expressing PDGFRβ$^+$/α$^+$ (PDPN$^+$) mesenchymal cells were detected in the thymic and LN capsule (data not shown) and as outer layers surrounding PDGFRβ$^+$/α$^-$ (PDPN$^-$) cells and CD31$^+$ endothelium of larger blood vessels throughout the thymus and in the LN medulla (Figures 2H–2K, arrows). Similarly, a population of PDGFRβ$^+$/α$^+$CD34$^+$ mesenchymal cells surrounded central arterioles in splenic white pulp areas (Figures S2D and S2E). Notably, PDPN$^-$ LNMC and TMC selectively expressed the endothelial cell regulator angiopoietin-1 (Fagiani and Christofori, 2013) (Figure 2L) while BP-3$^-$PDPN$^+$ LNMC and TMC were major sources of VEGF, IGF, and FGF family members with vasculogenic/angiogenic potential (Contois et al., 2012; Das et al., 2013; Lee et al., 2000; Lohela et al., 2009; Oh et al., 2012; Presta et al., 2005; Shigematsu et al., 1999; Zhang et al., 2012) (Figures 2L and 2M). Further, BP-3$^-$PDPN$^+$ TMC, but not PDPN$^-$ TMC, expressed mRNA for IGF-1, IGF-2, FGF-7, and FGF-10, which have been implicated as mesenchymal-dependent regulators of TEC growth (Jenkinson et al., 2007; Revest et al., 2001) (Figures 2L and 2M). To assess the role of lymphocytes in the generation and/or maintenance of lymphoid mesenchymal cells, the TMC and LMNC subset composition of *Rag1*$^{-/-}$ mice was assessed (Figures S2F–S2L). BP3$^-$PDPN$^+$ and PDPN$^-$ TMC were found at normal ratios in *Rag1*$^{-/-}$ mice (Figures S2F–S2H). Among the three major LNMC subsets, *Rag1*$^{-/-}$ mice displayed a marked decrease in the proportion of BP-3$^+$PDPN$^+$ LNMC, a slight but significant increase in BP-3$^-$PDPN$^+$CD34$^+$ LNMC, and a slight decrease in PDPN$^-$ LNMC compared with control mice (Figures S2I and S2J). Further remaining BP-3$^+$PDPN$^+$ LNMC in *Rag1*$^{-/-}$ mice expressed reduced levels of BP3 as well as intracellular CCL21 (Figures S2J–S2L).

Adult Adipose-Derived CD34$^+$ Adventitial Cells Can Differentiate into Multiple Lymphoid Stroma-like Subsets

We next determined whether BP-3$^-$PDPN$^+$PDGFRβ$^+$/α$^+$CD34$^+$ cells were also present in adventitial vascular niches of murine extra-lymphoid tissues. Indeed, PDGFRα$^+$CD34$^+$ cells were observed surrounding αSMA$^+$ vascular smooth muscle cell (VSMC)-containing tunica media of the aorta as well as within the vascular niche of adipose tissue and intestine (Figures 3A and 3B, data not shown). Flow cytometry analysis of CD45$^-$CD31$^-$ fractions in digested adipose tissue demonstrated, as in lymphoid tissues, that PDGFRα$^+$CD34$^+$ adventitial cells expressed PDGFRβ, PDPN, but not BP-3, and they represented a distinct compartment from PDGFRβ$^+$/α$^-$ITGA7$^+$Esam-1$^+$ cells (Figures 3C and 3D). Since purified adult human CD34$^+$ adventitial cells have previously been reported to contain clonal progenitors with tri-lineage adipogenic, chondrogenic, and osteogenic potential in vitro (Corselli et al., 2012), we next assessed whether murine CD34$^+$ adventitial cells could generate lymphoid stromal subsets. Flow cytometry analysis of adipose tissue CD34$^+$ adventitial cells demonstrated that these cells were heterogeneous in their expression of ICAM-1 (Figure 3D), a marker induced on PDGFRα$^+$PDPN$^+$ LNMC during LN ontogeny (Bénézech et al., 2010). We thus sorted EYFP$^+$ ICAM-1$^{-/lo}$ CD34$^+$ adventitial cells from digested subcutaneous fat of 2- to 5-month-old *Eyfp*-Rosa26 mice (for gating strategy see Figure S3A) and re-aggregated these cells with single cell suspensions obtained from wild-type E19 mesenteric LN or E15 thymus, and 36–48 hr later, resulting re-aggregate LN organ cultures (RLOC) and re-aggregate thymus organ cultures (RTOC) were engrafted under the kidney capsule of wild-type recipient mice (Figure 3E). Consistent with previous studies (Bénézech et al., 2012; Wong et al., 2014), 3 weeks after grafting, RLOC had adopted a LN structure containing populations of mature T and B cells segregated into T and B cell zones (Figures S3B and S3C) and with all LNMC subsets (Figure 2) present within the YFP$^-$ stromal cell compartment (Figures S3D and S3E). In contrast, RTOC contained CD4$^+$CD8$^+$ double-positive (DP) as well as CD8$^+$ and CD4$^+$ single-positive (SP) thymocytes (Figure S3C), and the YFP$^-$ stromal cell compartment of RTOC grafts was composed of subsets characteristic of the thymic stroma (Figures S3D and S3E). EYFP$^+$ cells in RLOC grafts could be divided into populations of PDPN$^-$PDGFRα$^-$ITGA7$^+$ and PDPN$^+$PDGFRα$^+$ cells, the latter subset consisting of a BP-3$^-$ and a BP-3$^+$ fraction (Figures 3F, 3G, and S3F) with EYFP$^+$BP-3$^+$PDPN$^+$ cells containing populations of MAdCAM-1$^+$ and CR1/2$^+$ cells (Figures 3F and 3G). Consistent with the distribution of ITGA7$^+$ pericytes and CD34$^+$ adventitial cells in nascent LNs, EYFP$^+$ITGA7$^+$ cells were found both inside and outside of the paracortical areas in the grafts in intimate association with CD31$^+$ blood vessels (Figure 3H), while EYFP$^+$CD34$^+$ cells integrated into the adventitial layer of larger blood vessels, in areas surrounding the paracortex, and in the capsule (Figure 3I). EYFP$^+$CR1/2$^+$ cells were selectively identified inside B

CD45$^-$EpCAM$^-$CD31$^-$PDPN$^+$ LNMC and TMC from 6- to 9-week-old mice were analyzed for expression of (A) CCL21, (B) MAdCAM-1, and (C) CR1/2. Data are representative of six (A), five (B), or three (C) experiments using pooled cells from one to six mice per experiment. rabIgG, rabbit IgG control. See also Figure S2. (E) αSMA and (F) Esam-1 expression by LNMC and TMC from 6- to 7-week-old mice. Data are representative of two (E) or three (F) experiments using pooled cells from two to six mice per experiment. (G) CD34 expression by PDPN$^+$ LNMC and TMC from 6- to 8-week-old mice. Data are representative of five experiments using pooled cells from two to five (LNMC) or one to two (TMC) mice per experiment. (A–C, E, G) Numbers are percentage of cells within indicated gates or (F) mean percentage (SD) of Esam-1$^+$ cells among PDPN$^-$ TMC. (A–G) LNMC; pooled inguinal, axillary, and brachial LNs.

(H and I) In situ localization of PDPN$^-$ (PDGFRβ$^+$/α$^-$; arrowheads) and PDPN$^+$ (PDGFRβ$^+$/α$^+$; arrows) mesenchymal cells in (H) the CMJ of the thymus and (I) medullary area of the inguinal LN. (J and K) In situ localization of BP3$^-$PDPN$^+$CD34$^+$ (PDGFRα$^+$CD34$^+$; arrows) mesenchymal cells in (J) the CMJ of the thymus and (K) medullary area of the inguinal LN. Sections from 2-week-old mice (H and I) or 7-week-old mice (J and K). Results are representative stains from (J) two or (H, I, K) three mice. Single color stains are shown on the right. See also Figure S2.

(M) Real-time PCR analysis of the indicated genes in PDPN$^-$ and PDPN$^+$ TMC from 2-week-old mice. Data are mean (SD) from three experiments using pooled cells from eight mice per experiment. *$p < 0.05$ and ***$p < 0.001$ (unpaired two-tailed Student's test).

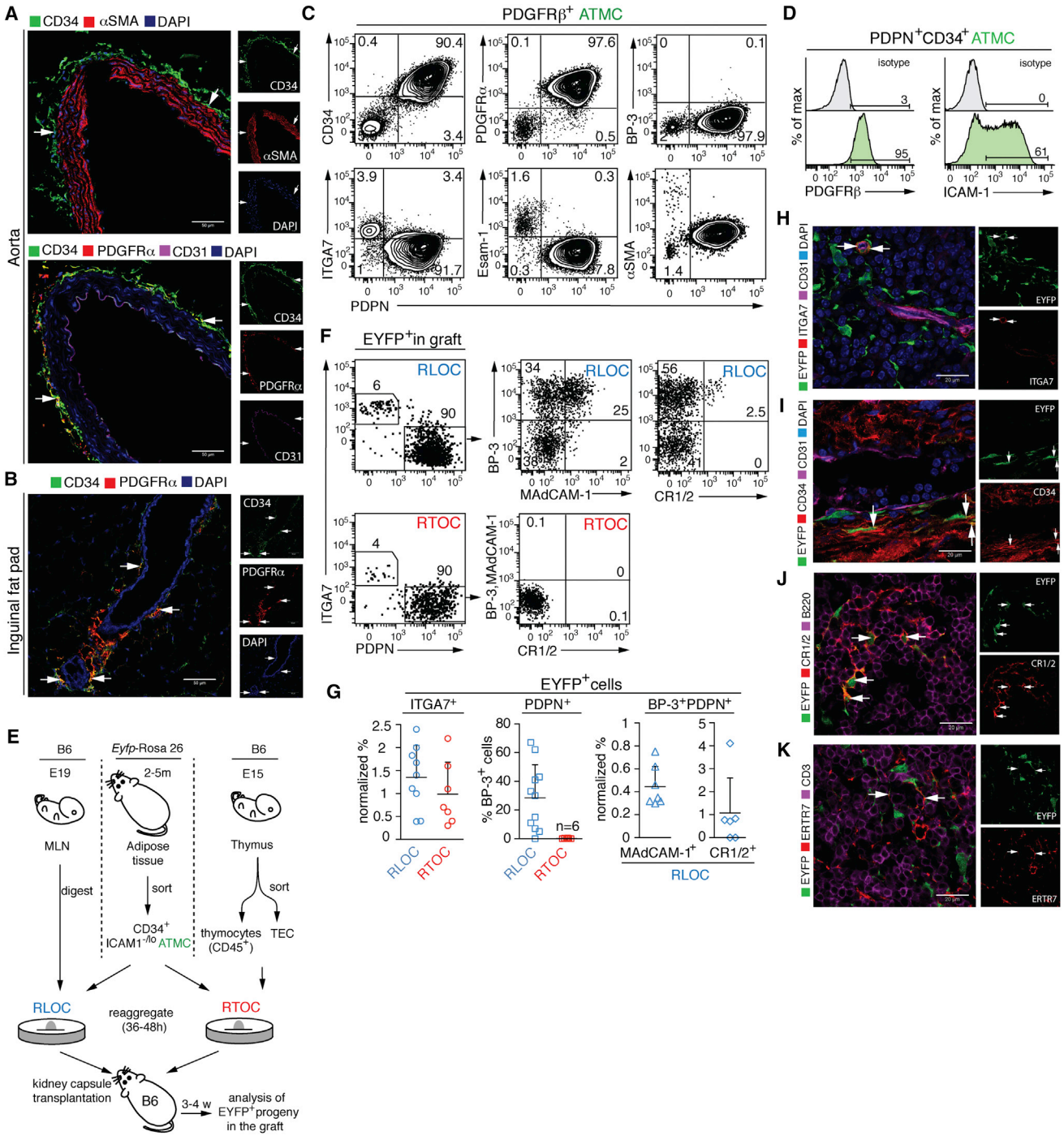

Figure 3. Adult Adipose-Derived CD34$^+$ Adventitial Cells Are Capable of Differentiating into Multiple Lymphoid Stromal-like Subsets

(A and B) Cryosections of the aorta (A) and inguinal fat pad (B) from an 11-week-old mouse were stained with indicated antibodies. Single color stains are shown on the right. Examples of PDGFRα$^+$CD34$^+$ adventitial cells (arrows).

(C and D) Phenotype of PDGFRβ$^+$ (C) or PDPN$^+$CD34$^+$ (D) CD45$^-$CD31$^-$ adipose tissue mesenchymal cells isolated from subcutaneous fat of 5- to 12-week-old mice. Numbers are percentage of cells within indicated gates. Representative plots from three experiments using pooled cells from (C) one to two or (D) one to six mice/experiment.

(E–G) RLOC and RTOC were spiked with EYFP$^+$ ICAM-1$^{-/lo}$ BP3$^-$PDPN$^+$CD34$^+$ Esam-1$^-$ adventitial cells from 2- to 5-month-old *Eyfp*-Rosa26 mice (for sorting strategy see Figure S3A), transplanted under the kidney capsule of 7- to 11-week-old wild-type mice and EYFP$^+$ cells in the grafts analyzed 3 to 4 weeks later. (C–E) ATMC, adipose tissue mesenchymal cells. (F) Representative plots pre-gated on indicated populations and (G) percentage of indicated EYFP$^+$ subsets. (G) Percentage of EYFP$^+$ PDPN$^-$ITGA7$^+$, MAdCAM-1$^+$, and CR1/2$^+$ cells was normalized to the percentage of corresponding subsets among EYFP$^-$

(legend continued on next page)

cell rich areas of the paracortex (Figure 3J), and consistent with the detection of EYFP$^+$BP3$^+$MAdCAM-1$^-$CR1/2$^-$ cells by flow cytometry, EYFP$^+$ cells were also found associated with ERTR7$^+$ reticular fibers in T cell-rich areas (Figure 3K). In marked contrast to RLOC grafts, EYFP$^+$ ICAM-1$^{-/lo}$ CD34$^+$ adventitial cells in RTOC grafts differentiated into PDPN$^-$ITGA7$^+$ cells but failed to differentiate into BP-3$^+$PDPN$^+$ subsets (Figures 3F and 3G). Collectively, these results indicate that adult ICAM-1$^{-/lo}$ CD34$^+$ adventitial cells contain precursors capable of giving rise to pericyte-, FRC-, MRC-, and FDC-like cells, and the differentiation capacity of these cells is dependent on the environmental context.

CD34$^+$ Thymic Adventitial Cells Contain Precursors with Lymphoid Stroma-like Subset Potential

To assess whether lymphoid-resident CD34$^+$ adventitial cells also display lymphoid stromal subset-like potential, we performed similar experiments with postnatal thymic BP3$^-$PDPN$^+$ cells (all of which express CD34; Figure 2G; data not shown). Analysis of Sox10Cre.Rosa*Eyfp* mice, in which neural crest (NC)-derived cells are indelibly marked with EYFP expression (Müller et al., 2008), demonstrated that both adult PDPN$^-$ and BP-3$^-$PDPN$^+$ TMC were of NC-origin (Figures S4A and S4B). RTOC grafts were thus spiked with EYFP$^+$BP-3$^-$PDPN$^+$ or EYFP$^+$PDPN$^-$Esam-1$^+$ TMC from 2- to 3-week-old Sox10Cre.Rosa*Eyfp* mice (Figure 4A), a time point when maximal numbers of EYFP$^+$PDPN$^-$Esam-1$^+$ TMC could be obtained (Figure S4C). Postnatal EYFP$^+$BP-3$^-$PDPN$^+$ TMC generated PDPN$^-$Esam-1$^+$ cells (Figures 4B and 4C) but failed to generate BP-3$^+$PDPN$^+$ cells in five of five independently generated RTOC grafts (Figure 4C). Conversely, EYFP$^+$PDPN$^-$Esam-1$^+$ TMC failed to differentiate into PDPN$^+$ cells (Figures 4B and 4C) and EYFP$^+$ cell recovery in those grafts was diminished (data not shown). We next tracked the expression of ICAM-1 by PDPN$^+$ TMC from E14.5 until 9 weeks of age (Figure 4D). At E14.5, PDPN$^+$ TMC were uniformly ICAM-1$^{-/lo}$, however, by birth, a subset of cells expressing an elevated level of ICAM-1 (hereafter called ICAM-1^{hi}) had emerged and the ICAM-1^{hi} to ICAM-1$^{-/lo}$ ratio within the PDPN$^+$ TMC compartment as well as the surface levels of ICAM-1 expressed by ICAM-1^{hi} cells continued to increase until 9 weeks (Figure 4D). These results suggested, similar to LNs (Bénézech et al., 2010), a maturation pathway for PDPN$^+$ TMC involving upregulation of ICAM-1 by ICAM-1$^{-/lo}$ precursors. To determine whether postnatal ICAM-1$^{-/lo}$ and ICAM-1^{hi} BP-3$^-$PDPN$^+$ thymic adventitial cells were capable of generating pericyte-like cells, EYFP$^+$ ICAM-1$^{-/lo}$ and ICAM-1^{hi} BP-3$^-$PDPN$^+$ TMC were isolated from 5-week-old Sox10Cre.Rosa*Eyfp* mice and used in RTOC grafting experiments (Figures 4A, 4E, and 4F). EYFP$^+$PDPN$^+$ cells in grafts spiked with ICAM-1$^{-/lo}$ and ICAM-1^{hi} BP-3$^-$PDPN$^+$ TMC were ICAM-1^{hi}, suggesting that postnatal ICAM-1$^{-/lo}$ BP-3$^-$PDPN$^+$ TMC contain precursors of ICAM-1^{hi} BP-3$^-$PDPN$^+$ TMC (Figure 4E). Both populations were capable of differentiating into PDPN$^-$Esam-1$^+$ cells, although ICAM-1$^{-/lo}$ BP-3$^-$PDPN$^+$ TMC appeared to do so less efficiently (Figures 4E and 4F). Finally, EYFP$^+$ ICAM-1$^{-/lo}$ BP-3$^-$PDPN$^+$CD34$^+$ thymic adventitial cells sorted from 9-week-old Sox10Cre.Rosa*Eyfp* or 5- to 6-week-old *Eyfp*-Rosa26 mice gave rise in two out of five RLOC grafts to BP-3$^+$PDPN$^+$ cells containing MAdCAM-1$^+$ cells at ratios similar to EYFP$^+$ cells in adipose-derived adventitial cell-spiked RLOC (Figures 3G, 4G, and 4H). Together, these data suggest that CD34$^+$ adventitial cells of adult lymphoid tissues also include progenitors with lymphoid stromal subset-like potential.

PDPN$^-$ and BP-3$^-$PDPN$^+$CD34$^+$ TMC Develop from a Common Anlage-Seeding Population

To gain insight into the ontogeny of Esam-1$^+$PDPN$^-$, BP-3$^-$PDPN$^+$CD34$^+$ LNMC/TMC, and BP-3$^+$PDPN$^+$ LNMC, we assessed the population dynamics of these subsets during embryonic development. At E13.5, the PDGFRβ$^+$ TMC compartment was composed almost entirely of PDPN$^+$PDGFRα$^+$CD34$^{-/lo}$Esam-1$^-$ cells (Figure 5A). By E14.5, all TMC remained CD34$^{-/lo}$ and a small population of PDPN$^+$PDGFRα$^-$Esam-1$^+$ cells had emerged. By E18.5, PDPN$^+$PDGFRα$^+$ cells expressed intermediate levels of CD34, while PDPN expression by the PDGFRα$^-$Esam-1$^+$ fraction decreased (Figure 5A). By 7 days post-birth, PDPN$^+$PDGFRα$^+$ cells were CD34$^+$ while PDGFRα$^-$Esam-1$^+$ cells were PDPN$^-$ (Figure 5A). Similar to embryonic TMC, E16.5 LNMC were all BP-3$^-$CD34$^{-/lo}$ and composed of a major PDPN$^+$PDGFRα$^+$ and a minor PDGFRα$^-$Esam-1$^+$ population (Figure 5B). Notably, the latter subset contained a PDPN$^+$ fraction, not present in age-matched inguinal fat pad (Figure 5C), which by 1 week post-birth had downregulated PDPN (data not shown). By E17.5, all LNMC remained CD34$^{-/lo}$ and a subset of BP-3$^+$PDPN$^+$PDGFRα$^+$ cells emerged, the proportion of which continued to increase until 1 week post-birth (Figure 5B). At E18.5, the remaining BP-3$^-$PDPN$^+$PDGFRα$^+$ cells expressed intermediate levels of CD34 (Figure 5B). By 1 week post-birth, a distinct population of BP-3$^-$PDPN$^+$PDGFRα$^+$CD34$^+$ cells had emerged (Figure 5B). Further analysis of LNMC subsets in adult Sox10Cre.Rosa*Eyfp* mice demonstrated that PDPN$^-$, BP-3$^-$PDPN$^+$, and BP-3$^+$PDPN$^+$ mesenchymal cells in cervical LNs are of NC-origin while similar subsets in LNs located in the trunk were EYFP$^-$ and thus not of NC origin (Figure S5). Collectively, these results suggested that Esam-1$^+$PDPN$^-$ pericytes in both the thymus and LNs arise via a PDPN$^+$PDGFRα$^-$ intermediate from BP-3$^-$PDPN$^+$PDGFRβ$^+$/α$^+$CD34$^{-/lo}$ cells that subsequently upregulate CD34. To assess this possibility, E13.5 thymic lobes from *Eyfp*-Rosa26 mice (Srinivas et al., 2001) were grafted under the kidney capsule of wild-type recipient mice, and the phenotype of EYFP$^+$ cells was assessed in the grafts 12 days later

CD45$^-$EpCAM$^-$CD31$^-$ (PDPN$^-$ITGA7$^+$) or CD45$^-$EpCAM$^-$CD31$^-$PDPN$^+$BP-3$^+$ (MAdCAM-1$^+$ and CR1/2$^+$) graft-derived mesenchymal cells. Each symbol represents data from one graft. Horizontal line, mean (SD).

(H–K) In situ localization of (H) EYFP$^+$ITGA7$^+$ pericyte-like cells (arrows), (I) EYFP$^+$CD34$^+$ adventitial-like cells (arrows), (J) EYFP$^+$CR1/2$^+$ FDC-like cells (arrows), and (K) EYFP$^+$ERTR7$^+$ T-zone FRC-like cells (arrows) in transplanted RLOC. Results are representative stains from three individual RLOC grafts. Single color stains are shown on the right.

See also Figure S3.

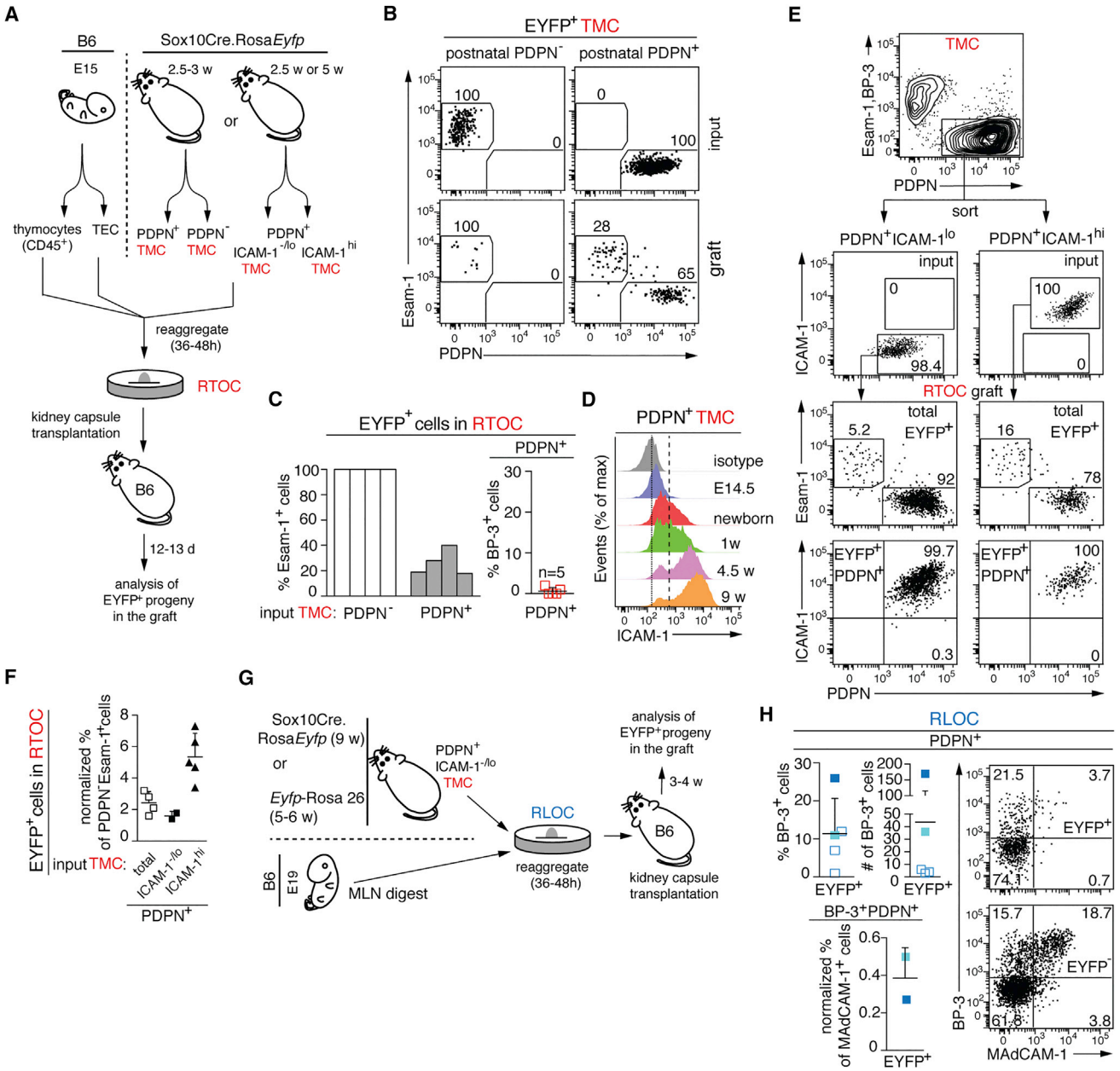

Figure 4. Postnatal Thymus-Derived CD34$^+$ Adventitial Cells Contain Precursors with Lymphoid Stroma-like Subset Potential

(A–C, E, F) RTOC were spiked with EYFP$^+$ TMC from 2.5- to 3-week-old (A–C) or 2.5- or 5-week-old (E and F) Sox10Cre.Rosa26*Eyfp* mice as indicated, transplanted under the kidney capsule of 7- to 10-week-old wild-type mice and EYFP$^+$ cells in the grafts analyzed 12–13 days later. (B and E) Representative plots pre-gated on indicated populations. (C and F) Percentage of indicated EYFP$^+$ subsets. (F) Data are normalized to the percentage of PDPN$^-$Esam-1$^+$ cells among EYFP$^-$CD45$^-$EpCAM$^-$CD31$^-$ mesenchymal cells in the graft.

(D) ICAM-1 expression by PDPN$^+$PDGFRα^+ TMC at indicated time points. Dotted vertical line shows the mean fluorescence intensity (MFI) of the isotype control and the dashed vertical line separates ICAM-1$^{-/lo}$ and ICAM-1^{hi} subsets. All time-points were analyzed on the same day. Data are representative results from three biological replicates per time-point using pooled cells from three (E14.5, newborn) or one (1 week, 4.5 weeks, 9 weeks) mice/replicate.

(G and H) RLOC were spiked with EYFP$^+$ ICAM-1$^{-/lo}$ BP3$^-$PDPN$^+$CD34$^+$Esam-1$^-$ TMC from 9-week-old Sox10Cre.Rosa26*Eyfp* or 5- to 6-week-old *Eyfp*-Rosa26 mice, transplanted under the kidney capsule of 5- to 9-week-old wild-type mice and EYFP$^+$ cells in the grafts analyzed 3–4 weeks later. (H) Representative plots pre-gated on total EYFP$^+$ or EYFP$^-$ CD45$^-$EpCAM$^-$CD31$^-$ cells and percentage and number of indicated EYFP$^+$ subsets. Percentage of EYFP$^+$MAdCAM-1$^+$ cells was normalized to the percentage of MAdCAM-1$^+$ cells among EYFP$^-$ CD45$^-$EpCAM$^-$CD31$^-$PDPN$^+$BP-3$^+$ graft-derived mesenchymal cells. (B, E, H) Numbers in the plots are percentage of cells within indicated gates, and (C, F, H) each bar or symbol represents data from a single graft. (H) Filled symbols of the same color denote the same graft in different graphs.

See also Figure S4.

(Figure 5D). The PDGFRβ$^+$ mesenchymal compartment in the grafts consisted mainly of EYFP$^+$ Esam-1$^+$PDPN$^-$ and PDPN$^+$CD34$^+$ cells (Figure 5E). To directly assess whether Esam-1$^+$PDPN$^-$ TMC could be generated from PDPN$^+$PDGFRα$^+$ embryonic thymic mesenchyme, EYFP$^+$ PDPN$^+$PDGFRα$^+$Esam-1$^-$ mesenchymal cells were sorted from E14.5 thymuses of Sox10Cre.Rosa*Eyfp* mice and re-aggregated with embryonic TEC and thymocytes. The RTOC were then grafted under the kidney capsule of wild-type recipient mice and the phenotype of EYFP$^+$ cells in the grafts was assessed after 10 days (Figure 5F). Consistent with results from E13.5 thymus transplantation, a large proportion of EYFP$^+$ cells recovered from the grafts were PDPN$^-$PDGFRα$^-$Esam-1$^+$ demonstrating the capacity of embryonic PDPN$^+$PDGFRβ$^+$/α$^+$CD34$^{-/lo}$Esam-1$^-$ TMC to give rise to Esam-1$^+$PDPN$^-$ cells (Figures 5G and 5H). We were unable to perform similar studies with embryonic BP-3$^-$PDPN$^+$PDGFRβ$^+$/α$^+$CD34$^{-/lo}$Esam-1$^-$ LNMC due to limited cell numbers. Further, when *Eyfp*-Rosa26 E16.5 inguinal LN anlagen was grafted under the kidney capsule of wild-type recipients only 3 out of 26 grafts recovered contained T and B cells, consistent with the inability of E15.5 inguinal LN to generate functional LN grafts due to insufficient number of CD3$^-$CD4$^+$ inducer cells (White et al., 2007). Only one of these contained sufficient LNMC for analysis, and the CD45$^-$CD31$^-$ compartment in this graft consisted almost exclusively of EYFP$^+$ cells and contained PDPN$^-$ITGA7$^+$, BP-3$^-$PDPN$^+$CD34$^+$ as well as BP-3$^+$PDPN$^+$ cells including CCL21$^+$ FRC-like cells (data not shown). Collectively, these results demonstrate that PDPN$^-$ and BP-3$^-$PDPN$^+$CD34$^+$ TMC originate from a common PDPN$^+$PDGFRβ$^+$/α$^+$CD34$^{-/lo}$Esam-1$^-$ subset of anlage-seeding precursors and suggest that LNMC subsets may originate from a phenotypically similar BP-3$^-$ precursor population.

LTβR Signaling Is Required for the Maturation/Maintenance of BP-3$^-$PDPN$^+$ TMC

Given previous evidence implicating a role for LTβR-signaling in the differentiation of FRC, MRC, and FDC (Chai et al., 2013; Katakai et al., 2008; Krautler et al., 2012), we finally sought to assess the role of the LTβR pathway in the development of Esam-1$^+$PDPN$^-$ and BP3$^-$PDPN$^+$ TMC, all of which express LTβR (Figure 6A). Consistent with a previously reported reduction in PDGFRα$^+$ TMC in *Lta*$^{-/-}$ and *Ltb*$^{-/-}$ mice (Gray et al., 2007), *Ltbr*$^{-/-}$ mice displayed a marked reduction in ICAM-1^{hi}VCAM-1$^+$PDPN$^+$ TMC while ICAM-1^{hi}VCAM-1$^-$, ICAM-1$^{-/lo}$ PDPN$^+$, and Esam-1$^+$PDPN$^-$ TMC compartments were unaffected (Figures 6B–6E). ICAM-1^{hi}VCAM-1$^-$ PDPN$^+$ TMC from *Ltbr*$^{-/-}$ mice also displayed reduced ICAM-1 expression indicative of a maturation defect (Figure 6F). Together, these results suggest that LTβR signaling is required for the maturation of the CD34$^+$ TMC compartment. ICAM-1^{hi}VCAM-1$^+$PDPN$^+$ TMC and ICAM-1 expression on these cells was unaffected in *Rag1*$^{-/-}$ mice (Figure 6G), indicating that DP and SP thymocytes were not a key source of LTβR ligands regulating CD34$^+$ TMC homeostasis.

DISCUSSION

Studies assessing the phenotype and heterogeneity of lymphoid mesenchymal cell compartments have relied heavily on in situ immunohistochemical analysis, and our understanding of the subset composition and specialized function of LNMC and TMC remains far from complete. Here, by combining detailed flow cytometry and global gene expression analysis in combination with in situ localization studies, we performed a comprehensive analysis of the mesenchymal subset composition in LNs and thymus that we believe provides an important framework for assessing mesenchymal functional specialization and for the interpretation of prior genetic reporter and Cre-mediated deletion strategies. Prior flow cytometry analysis of LNMC has suggested that PDPN$^+$ LNMC contain MAdCAM-1$^+$ MRC, CR1/CR2$^+$ FDC and MAdCAM-1$^-$CR1/CR2$^-$ FRC (Malhotra et al., 2012). Consistent with these findings, we demonstrate that all three subsets are present within the PDPN$^+$ fraction of LNMC, with FRC positively identified by their expression of intracellular CCL21, and these populations can be collectively distinguished by their co-expression of BP-3. While BP-3$^+$PDPN$^+$ cells were absent from the TMC compartment, we identified two mesenchymal subsets common to both the thymus and LNs; a PDPN$^-$PDGFRβ$^+$/α$^-$Esam-1$^+$ITGA7$^+$ mesenchymal subset containing contractile and non-contractile pericytes and a population of BP-3$^-$PDPN$^+$PDGFRβ$^+$/α$^+$CD34$^+$ mesenchymal cells. Both subsets localized within distinct locations in the vascular niche with the former cells, consistent with their pericyte-associated gene expression signature, intimately associating with the vascular endothelium and the latter forming the adventitia surrounding these cells. Previous studies have demonstrated that CD34 is expressed by adventitial cells within human adipose tissue, skeletal muscle, pancreas, and lung (Corselli et al., 2012; Lin et al., 2008) as well as murine aorta (Hu et al., 2004), and we demonstrate here that CD34$^+$ adventitial cells are also present within murine adipose tissue and small intestine indicating that CD34 may represent a conserved marker to identify adventitial cells within the vascular niche. Notably, lymphoid tissue BP-3$^-$PDPN$^+$CD34$^+$ adventitial mesenchymal cells and PDPN$^-$ITGA7$^+$ pericytes expressed a distinct array of endothelial regulatory and angiogenic factors suggesting that these subsets play partially non-redundant roles in supporting vascular endothelial cell homeostasis in these tissues.

Utilizing kidney capsule transplantation of spiked lymphoid organ re-aggregates, we provide evidence that adult CD34$^+$ adventitial cells at a population level are capable of giving rise to multiple lymphoid stroma-like subsets. These results are consistent with prior observations that adult adipose-derived PDGFRα$^+$PDPN$^+$ stromal cells generate MAdCAM-1$^+$ progeny as well as ERTR7$^+$ FRC-like networks in transplanted LN re-aggregate grafts (Bénézech et al., 2012), and adult PDGFRβ$^+$ adipose-derived cells give rise to CR1/CR2$^+$ FDC-like cells following grafting and immunization (Krautler et al., 2012). Phenotypic and functional equivalents of LNMC subsets arise ectopically in multiple adult organs as part of organized tertiary lymphoid organs (TLO) that develop in association with chronic inflammation and cancer (Neyt et al., 2012). While the identity of the mesenchymal TLO precursors remains unclear, our findings suggest that CD34$^+$ adventitial cells may be a potential source of TLO stromal progenitors in extra-lymphoid tissues. Indeed, lymphoid neo-genesis is observed in association with

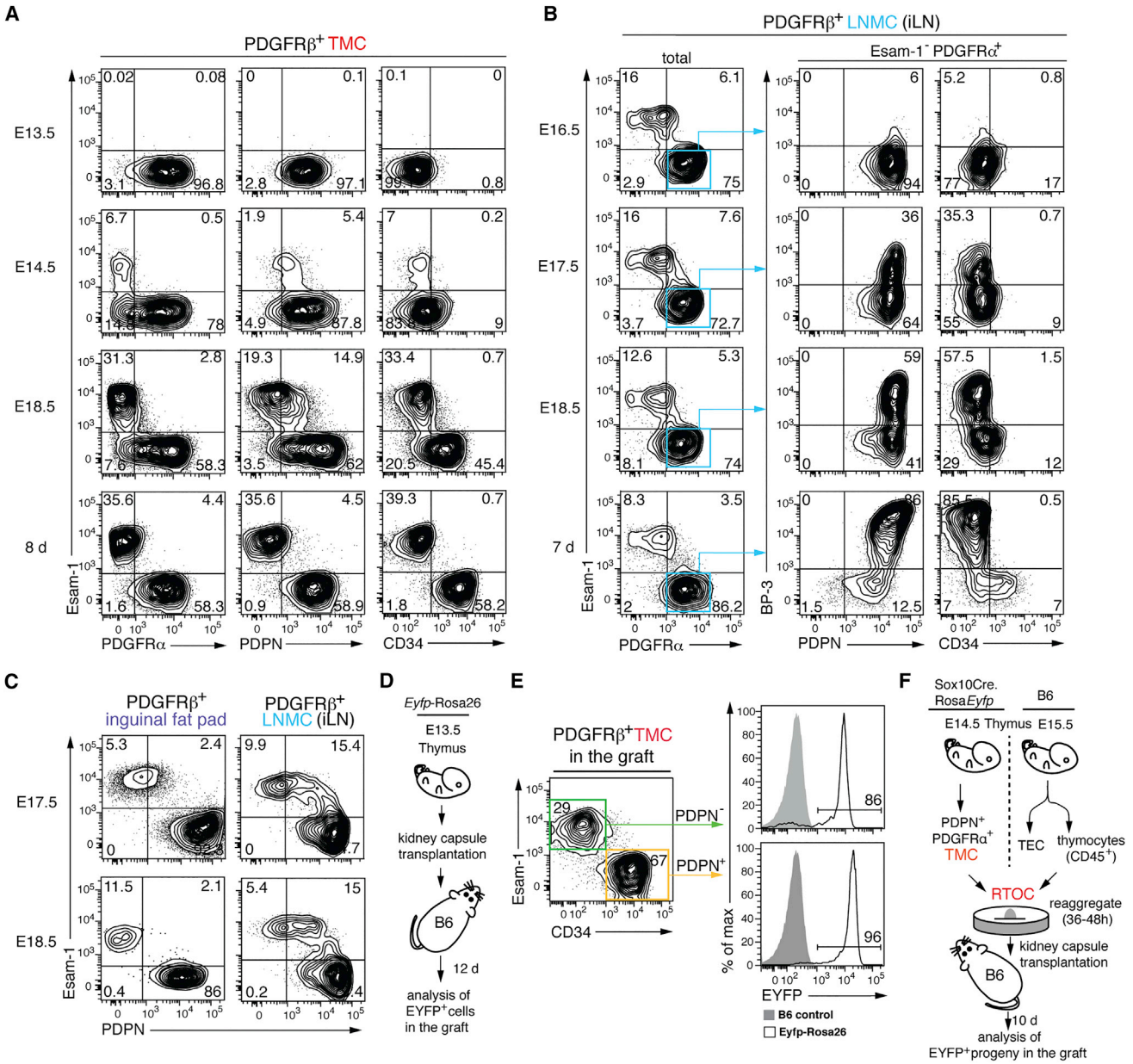

(legend on next page)

blood vessels in lungs of patients with idiopathic pulmonary hypertension (Perros et al., 2012) and within the adventitia of atherosclerotic plague-burdened aorta of aged *Apoe*$^{-/-}$ mice (Gräbner et al., 2009).

While pericyte-like cells were generated in transplanted RTOC and RLOC, only the latter supported the development of B-zone CR1/2^{+} FDC-like, T-zone ERTR7^{+} FRC-like, and MAdCAM-1^{+} MRC-like BP3^{+}PDPN^{+} subsets. Collectively, these results suggest that differences in thymic and LN mesenchymal cell subset composition are not a result of cell intrinsic properties of seeding stromal populations but rather governed by tissue-specific signals mesenchymal cells receive within their respective environments. While the tissue-derived signals that allow BP-3^{+}PDPN^{+} mesenchymal cell subset generation in LNs, but not thymus, remain to be fully elucidated, we demonstrate that *Rag-1*$^{-/-}$ mice have reduced proportions of BP-3^{+}PDPN^{+} LNMC and that remaining BP-3^{+}PDPN^{+} LNMC in these mice display reduced expression of BP-3 and CCL21. Consistent with these findings, SCID and/or *Rag-2*$^{-/-}$ mice have previously been shown to lack FDC and to display a marked reduction in PDPN^{+}MAdCAM-1^{+} LNMC (Fletcher et al., 2011; Gonzalez et al., 1998). These results also suggest that a lack of a particular T and/or B cell subset cannot alone account for the absence of BP-3^{+}PDPN^{+} cells in the thymus and in RTOC grafts. We speculate that the differential generation of BP-3^{+}PDPN^{+} cells in these organs could be additionally promoted by the presence of specific inhibitory factors. In this regard, it is of interest to note that progressive reduction in TEC, as occurs in FoxN1-Cre.*Dicer*$^{fl/fl}$ mice (Zuklys et al., 2012), leads to thymic induction of a LN-like environment including generation of CD21^{+} FDC-like and ERTR7^{+} FRC-like mesenchymal networks in areas devoid of TEC.

Our studies on the kinetics of embryonic lymphoid tissue development suggest that CD34^{+} adventitial cells arise in the thymus in the late embryo and in the LNs postnatally. Further, we demonstrate in the thymus that these cells develop, along with pericytes, from PDPN^{+}PDGFRβ^{+}/α^{+}CD34$^{-/lo}$ anlage-seeding mesenchymal precursors. Pericytes have been shown to originate from both mesoderm and neural crest (Armulik et al., 2011), however, the developmental relationship of pericytes to other mesenchymal populations has remained unclear. Our findings suggest that lymphoid-associated pericytes do not arise from CD34^{+} adventitia during ontogeny but that the latter cells may contribute to pericyte turnover and homeostasis in postnatal tissues.

In conclusion, our comprehensive assessment of lymphoid stromal cell functional heterogeneity and ontogeny led to the identification of lymphoid CD34^{+} cells as a common constituent of the vascular niche, distinct from pericytes, FRC, MRC, and FDC and showed that CD34^{+} adventitial cells at the population level display lymphoid stroma-like progenitor potential. While future experiments are required to assess the multi-potent progenitor potential of individual CD34^{+} adventitial cells, we believe our findings provide an important framework for future studies assessing stromal subset functionality and ontogeny not only during the initiation of adaptive immunity but also in pathological settings such as cancer, obesity, vascular disease, and chronic inflammation.

EXPERIMENTAL PROCEDURES

Mice

C57BL/6 mice, *Rag1*$^{-/-}$ mice, *Eyfp*-Rosa26 mice (Srinivas et al., 2001), and Sox10Cre.Rosa26*Eyfp* mice (Müller et al., 2008) were bred and maintained at the Biomedical Centre Animal Facility (Lund University, Lund, Sweden). *Ltbr*$^{-/-}$ and *Ltbr*$^{+/(+/-)}$ mice were housed in the Biomedical Services Unit at the University of Birmingham, UK. Day of vaginal plug detection was designated as day 0.5 of gestation. All animal procedures were approved by the Lund/Malmö Animal Ethics Committee.

Flow Cytometry and Cell Sorting

Flow cytometry was performed with antibodies (Table S1) according to standard procedures. Dead cells (identified as propidium iodide^{+} or using LIVE/DEAD Violet Fixable Dead Cell Staining Kit; both from Invitrogen) and cell aggregates (identified on FSC-A versus FSC-W scatter plots) were excluded from all analyses. Data acquisition was performed on a FACSAria or LSRII (BD Biosciences) and analyzed using FlowJo software (Tree Star). For analysis of αSMA and CCL21 expression, surface-labeled cell suspensions were fixed and permeabilized using the Foxp3 Staining Buffer Set (eBioscience) or 4% PFA and 0.1% saponin, respectively, followed by staining with FITC-anti-αSMA antibody or consecutive incubations with rabbit anti-CCL21 antibody and Alexa Fluor 647-goat anti-rabbit IgG secondary antibody. Sorting was performed on a FACSAria (BD Biosciences).

Immunofluorescence Staining

Cryosections (7–8 μm) from snap frozen or paraformaldehyde-fixated tissues were stained with antibodies (Table S2) using standard protocols and as detailed in the Supplemental Experimental Procedures. EYFP expressing cells were identified following incubation with a polyclonal chicken anti-GFP antibody (Aves Labs) and Alexa488 conjugated donkey anti-chicken secondary antibody (Jackson ImmunoResearch). Images were acquired with LSM 750 confocal microscope and analyzed using ZEN software (both from Carl Zeiss MicroImaging).

Figure 5. PDPN^{-} and BP-3^{-}PDPN^{+}CD34^{+} TMC Derive from a Common Anlage-Seeding Population

(A–C) PDGFRβ^{+} thymic (A), inguinal LN (B and C), and inguinal fat pad (C) mesenchymal cell subset composition was assessed at indicated time points. Numbers in the plots are percentage of cells in each quadrant. (A) Data are representative plots from three experiments using pooled thymic cells from two to three mice per experiment. (B) Data are representative of pooled cells from five (day 7), six (E17.5), or eight (E16.5) mice or representative of three experiments (E18.5) using pooled cells from six to nine mice per experiment. (C) Data are representative of pooled cells from five to six mice (E17.5) or of two experiments using fat pad cells from individual mice or pooled inguinal LN cells from six to nine mice per experiment.

(D and E) Thymic lobes from E13.5 *Eyfp*-Rosa26 mice were transplanted under the kidney capsule of 7-week-old wild-type recipients and PDGFRβ^{+} mesenchymal cells in the grafts analyzed 12 days later. (E) Representative plot and percentage of EYFP^{+} cells among PDPN^{-}Esam-1^{+} (PDPN^{-}) and PDPN^{+}CD34^{+} (PDPN^{+}) mesenchymal populations from three individual grafts. Numbers in the plots are percentage of cells within indicated gates.

(F–H) RTOC were spiked with EYFP^{+} TMC from E14.5 Sox10Cre.Rosa*Eyfp* mice as indicated, transplanted under the kidney capsule of 7- to 10-week-old wild-type mice and EYFP^{+} cells in the grafts analyzed 10 days later. (G) Representative plots and (H) percentage of PDPN^{-}Esam-1^{+} cells among total EYFP^{+} cells in the grafts. (G) Numbers in the plots are percentage of cells within each gate. (H) Each bar represents data from an individual graft.

See also Figure S5.

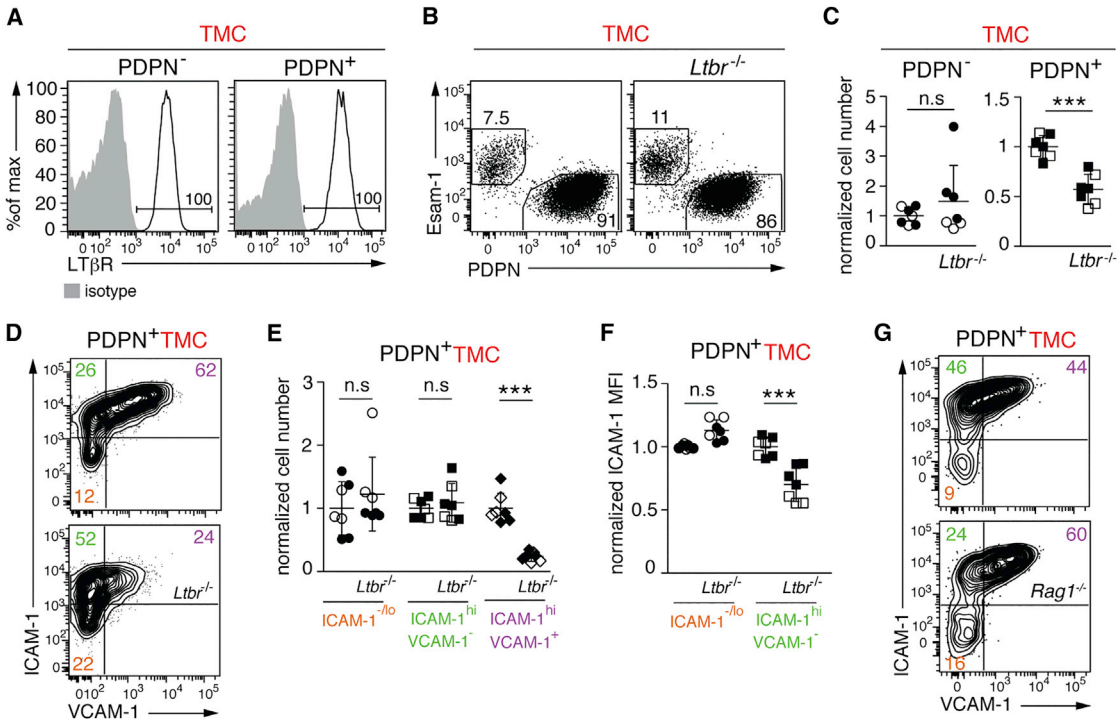

Figure 6. LTβR Signaling Plays a Role in the Maturation/Maintenance of BP-3⁻PDPN⁺ TMC

(A) PDPN⁻ and PDPN⁺ TMC from 2-week-old mice were analyzed for the expression of LTβR by flow cytometry. Shown are histogram plots representative of two biological replicates using pooled cells from two mice/replicate.

(B–F) Phenotype of PDGFRβ⁺ (B and C) or PDGFRβ⁺PDPN⁺ (D and F) mesenchymal subsets in the thymus of 5-week-old *Ltbr*$^{-/-}$ or littermate control mice. (B and D) Representative plots with numbers representing percentage of cells within indicated gates. (C and E) Cell numbers (mean, SD) and (F) mean fluorescence intensity of ICAM-1 expression in indicated TMC subsets from two independent experiments (filled and open symbols) with each symbol representing an individual mouse. (C, E, F) For normalization of cell number (C and E) or ICAM-1 expression (F), the mean value for each TMC subset in the control group was set to 1. The value for each individual mouse (control or *Ltbr*$^{-/-}$) was then divided by this mean. ***$p < 0.001$ (two-tailed Mann-Whitney test).

(G) Representative plots of ICAM-1 and VCAM-1 expression on PDGFRβ⁺PDPN⁺ TMC from 7 w old *Rag1*$^{-/-}$ and age-matched control mice. Results are representative plots from five mice/group from two independent experiments. Numbers in plots are percentage of cells within indicated quadrants.

Cell Isolation

Cell suspensions of thymus, LNs, and RTOC/RLOC grafts were prepared with liberase TM (0.32 Wunsch U ml^{-1}, Roche Diagnostics) and DNase I (50 Kunitz U ml^{-1}, Sigma-Aldrich) as previously described (Sitnik et al., 2012). For time course analysis of inguinal LN stroma, embryonic and early postnatal tissue was digested with collagenase P (1 mg ml^{-1}, Roche Diagnostics) and DNase I (50 Kunitz U ml^{-1}, Sigma-Aldrich) at 37°C for 45 min. Stromal cells were enriched by immunomagnetic depletion of CD45⁺ cells by MACS (Miltenyi Biotech) and thereafter stained with antibodies for analysis and cell sorting. Isolation of adipose tissue stromal vascular fraction (SVF) was performed as described (Church et al., 2014) with modifications. Briefly, subcutaneous adipose tissue was digested with liberase TM (0.32 Wunsch U ml^{-1}, Roche Diagnostics) and DNase I (50 Kunitz U ml^{-1}, Sigma-Aldrich) in high-glucose GlutaMAX-supplemented DMEM with 10 mM HEPES (Invitrogen) and 4% fatty acid-free BSA (Sigma-Aldrich) at 37°C for 55 min using an orbital shaker (350 rpm). The suspension was passed through a 100 μm nylon mesh filter (BD Biosciences), and the floating adipocyte fraction was removed by centrifugation at 400 × *g* for 6 min. The resulting SVF pellet was sequentially filtered through a 70 μm and a 40 μm filter.

RTOC and RLOC

For RTOC, EpCAM⁺CD45⁻ TEC (2.5–3.5 × 10^5 cells/RTOC) and CD45⁺ thymocytes (0.75–1.8 × 10^5 cells/RTOC) were sorted from single cell suspensions of 0.5% trypsin-EDTA (Invitrogen) digested E14.5–E15.5 thymi and re-aggregated with EYFP⁺ TMC (0.13–0.72 × 10^5 cells/graft) or ATMC (0.5–1 × 10^5 cells/graft). For RLOC, E19.5 mesenteric LNs were digested with collagenase P (1 mg ml^{-1}) and DNase I (50 Kunitz U ml^{-1}, Sigma-Aldrich) at 37°C for 45 min and resulting single-cell suspensions (5–7 × 10^5 cells per re-aggregate) combined with EYFP⁺ cells as described above. Cell suspensions were then used to establish RTOC and RLOC as previously described (Bénézech et al., 2012; White et al., 2008), incubated in 5% CO_2 at 37°C for 1–2 days and grafted under the kidney capsule of 5- to 12-week-old wild-type female recipients.

Real-Time RT-PCR

For analysis of 2-week-old TMC subsets, total RNA was extracted from 5–7 × 10^4 sorted cells using RNeasy Micro Kit (QIAGEN), reverse transcribed with SuperScript III and a 1:1 mixture of oligo-dT and random oligonucleotide hexamers (all from Invitrogen). Quantitative PCR was performed using Maxima SYBR Green qPCR Master Mix (Fisher Scientific) in a MyiQ Single Color-Real-Time PCR detection System (Bio-Rad). Gene expression was calculated using comparative dC_T method and normalized to *Gapdh*. Primer sequences are listed in Table S3.

Microarray Analysis

RNA was prepared from TMC and LNMC (pooled inguinal, brachial, and axillary LN) subsets sorted from 3 (TMC) and 10–11 (LNMC) 2-week-old mice per experiment. Isolated RNA from three individual experiments was amplified and prepared for hybridization to the Affymetrix Mouse Gene 1.1 ST Array in a genomics core facility: Center of Excellence for Fluorescent Bioanalytics (KFB, University of Regensburg, Germany) and analyzed as described in the Supplemental Experimental Procedures.

Statistical Analyses

Statistical analysis was performed using unpaired two-tailed Student's test or two-tailed Mann-Whitney non-parametric test as indicated (*$p < 0.05$, **$p < 0.01$, ***$p < 0.001$).

ACCESSION NUMBERS

The accession number for the microarray data reported in this paper is NCBI GEO: GSE76974.

SUPPLEMENTAL INFORMATION

Supplemental Information includes Supplemental Experimental Procedures, five figures, and three tables and can be found with this article online at http://dx.doi.org/10.1016/j.celrep.2016.02.033.

AUTHOR CONTRIBUTIONS

K.M.S. and W.W.A. conceived of and designed the study. K.M.S., K.W., H.U.-H., and K.K. performed experiments. H.W. analyzed microarray data. A.J.W. contributed key technical knowhow. G.A. contributed key technical and intellectual knowhow. K.M.S., K.K., and W.W.A. were involved in critical discussions throughout. K.M.S. and W.W.A. wrote the paper.

ACKNOWLEDGMENTS

We would like to thank Drs. Jorge Caamano and Nguyet-Thin Luu, Birmingham University for providing *Eyfp*-Rosa26 adipose tissue and together with Dr. W. Jenkinson, Birmingham University providing *Ltbr*$^{-/-}$ thymi, and A-C. Selberg for animal care. This work was supported by grants from the Swedish Natural Science Research Council, the Danish Medical Research Council, the Lundbeckfonden (R155-2014-4184), the Kocks, Österlund, and IngaBritt and Arne Lundbergs Foundations, and the Royal Physiographic Society.

Received: August 18, 2015
Revised: November 30, 2015
Accepted: February 2, 2016
Published: March 3, 2016

REFERENCES

Armulik, A., Genové, G., and Betsholtz, C. (2011). Pericytes: developmental, physiological, and pathological perspectives, problems, and promises. Dev. Cell *21*, 193–215.

Bénézech, C., White, A., Mader, E., Serre, K., Parnell, S., Pfeffer, K., Ware, C.F., Anderson, G., and Caamaño, J.H. (2010). Ontogeny of stromal organizer cells during lymph node development. J. Immunol. *184*, 4521–4530.

Bénézech, C., Mader, E., Desanti, G., Khan, M., Nakamura, K., White, A., Ware, C.F., Anderson, G., and Caamaño, J.H. (2012). Lymphotoxin-β receptor signaling through NF-κB2-RelB pathway reprograms adipocyte precursors as lymph node stromal cells. Immunity *37*, 721–734.

Chai, Q., Onder, L., Scandella, E., Gil-Cruz, C., Perez-Shibayama, C., Cupovic, J., Danuser, R., Sparwasser, T., Luther, S.A., Thiel, V., et al. (2013). Maturation of lymph node fibroblastic reticular cells from myofibroblastic precursors is critical for antiviral immunity. Immunity *38*, 1013–1024.

Chang, J.E., and Turley, S.J. (2015). Stromal infrastructure of the lymph node and coordination of immunity. Trends Immunol. *36*, 30–39.

Church, C.D., Berry, R., and Rodeheffer, M.S. (2014). Isolation and study of adipocyte precursors. Methods Enzymol. *537*, 31–46.

Contois, L.W., Nugent, D.P., Caron, J.M., Cretu, A., Tweedie, E., Akalu, A., Liebes, L., Friesel, R., Rosen, C., Vary, C., and Brooks, P.C. (2012). Insulin-like growth factor binding protein-4 differentially inhibits growth factor-induced angiogenesis. J. Biol. Chem. *287*, 1779–1789.

Corselli, M., Chen, C.W., Sun, B., Yap, S., Rubin, J.P., and Péault, B. (2012). The tunica adventitia of human arteries and veins as a source of mesenchymal stem cells. Stem Cells Dev. *21*, 1299–1308.

Das, S.K., Bhutia, S.K., Azab, B., Kegelman, T.P., Peachy, L., Santhekadur, P.K., Dasgupta, S., Dash, R., Dent, P., Grant, S., et al. (2013). MDA-9/syntenin and IGFBP-2 promote angiogenesis in human melanoma. Cancer Res. *73*, 844–854.

Fagiani, E., and Christofori, G. (2013). Angiopoietins in angiogenesis. Cancer Lett. *328*, 18–26.

Fletcher, A.L., Malhotra, D., Acton, S.E., Lukacs-Kornek, V., Bellemare-Pelletier, A., Curry, M., Armant, M., and Turley, S.J. (2011). Reproducible isolation of lymph node stromal cells reveals site-dependent differences in fibroblastic reticular cells. Front. Immunol. *2*, 35.

Girard, J.P., Moussion, C., and Förster, R. (2012). HEVs, lymphatics and homeostatic immune cell trafficking in lymph nodes. Nat. Rev. Immunol. *12*, 762–773.

Gonzalez, M., Mackay, F., Browning, J.L., Kosco-Vilbois, M.H., and Noelle, R.J. (1998). The sequential role of lymphotoxin and B cells in the development of splenic follicles. J. Exp. Med. *187*, 997–1007.

Gordon, J., and Manley, N.R. (2011). Mechanisms of thymus organogenesis and morphogenesis. Development *138*, 3865–3878.

Gräbner, R., Lötzer, K., Döpping, S., Hildner, M., Radke, D., Beer, M., Spanbroek, R., Lippert, B., Reardon, C.A., Getz, G.S., et al. (2009). Lymphotoxin beta receptor signaling promotes tertiary lymphoid organogenesis in the aorta adventitia of aged ApoE-/- mice. J. Exp. Med. *206*, 233–248.

Gray, D.H., Tull, D., Ueno, T., Seach, N., Classon, B.J., Chidgey, A., McConville, M.J., and Boyd, R.L. (2007). A unique thymic fibroblast population revealed by the monoclonal antibody MTS-15. J. Immunol. *178*, 4956–4965.

Hu, Y., Zhang, Z., Torsney, E., Afzal, A.R., Davison, F., Metzler, B., and Xu, Q. (2004). Abundant progenitor cells in the adventitia contribute to atherosclerosis of vein grafts in ApoE-deficient mice. J. Clin. Invest. *113*, 1258–1265.

Jenkinson, W.E., Rossi, S.W., Parnell, S.M., Jenkinson, E.J., and Anderson, G. (2007). PDGFRalpha-expressing mesenchyme regulates thymus growth and the availability of intrathymic niches. Blood *109*, 954–960.

Katakai, T., Suto, H., Sugai, M., Gonda, H., Togawa, A., Suematsu, S., Ebisuno, Y., Katagiri, K., Kinashi, T., and Shimizu, A. (2008). Organizer-like reticular stromal cell layer common to adult secondary lymphoid organs. J. Immunol. *181*, 6189–6200.

Krautler, N.J., Kana, V., Kranich, J., Tian, Y., Perera, D., Lemm, D., Schwarz, P., Armulik, A., Browning, J.L., Tallquist, M., et al. (2012). Follicular dendritic cells emerge from ubiquitous perivascular precursors. Cell *150*, 194–206.

Lee, O.H., Bae, S.K., Bae, M.H., Lee, Y.M., Moon, E.J., Cha, H.J., Kwon, Y.G., and Kim, K.W. (2000). Identification of angiogenic properties of insulin-like growth factor II in in vitro angiogenesis models. Br. J. Cancer *82*, 385–391.

Lin, G., Garcia, M., Ning, H., Banie, L., Guo, Y.L., Lue, T.F., and Lin, C.S. (2008). Defining stem and progenitor cells within adipose tissue. Stem Cells Dev. *17*, 1053–1063.

Link, A., Vogt, T.K., Favre, S., Britschgi, M.R., Acha-Orbea, H., Hinz, B., Cyster, J.G., and Luther, S.A. (2007). Fibroblastic reticular cells in lymph nodes regulate the homeostasis of naive T cells. Nat. Immunol. *8*, 1255–1265.

Lohela, M., Bry, M., Tammela, T., and Alitalo, K. (2009). VEGFs and receptors involved in angiogenesis versus lymphangiogenesis. Curr. Opin. Cell Biol. *21*, 154–165.

Malhotra, D., Fletcher, A.L., Astarita, J., Lukacs-Kornek, V., Tayalia, P., Gonzalez, S.F., Elpek, K.G., Chang, S.K., Knoblich, K., Hemler, M.E., et al.; Immunological Genome Project Consortium (2012). Transcriptional profiling of stroma from inflamed and resting lymph nodes defines immunological hallmarks. Nat. Immunol. *13*, 499–510.

Mori, K., Itoi, M., Tsukamoto, N., and Amagai, T. (2010). Foxn1 is essential for vascularization of the murine thymus anlage. Cell. Immunol. *260*, 66–69.

Müller, S.M., Stolt, C.C., Terszowski, G., Blum, C., Amagai, T., Kessaris, N., Iannarelli, P., Richardson, W.D., Wegner, M., and Rodewald, H.R. (2008). Neural crest origin of perivascular mesenchyme in the adult thymus. J. Immunol. *180*, 5344–5351.

Neyt, K., Perros, F., GeurtsvanKessel, C.H., Hammad, H., and Lambrecht, B.N. (2012). Tertiary lymphoid organs in infection and autoimmunity. Trends Immunol. *33*, 297–305.

Odaka, C. (2009). Localization of mesenchymal cells in adult mouse thymus: their abnormal distribution in mice with disorganization of thymic medullary epithelium. J. Histochem. Cytochem. *57*, 373–382.

Oh, S.H., Kim, W.Y., Lee, O.H., Kang, J.H., Woo, J.K., Kim, J.H., Glisson, B., and Lee, H.Y. (2012). Insulin-like growth factor binding protein-3 suppresses vascular endothelial growth factor expression and tumor angiogenesis in head and neck squamous cell carcinoma. Cancer Sci. *103*, 1259–1266.

Perros, F., Dorfmüller, P., Montani, D., Hammad, H., Waelput, W., Girerd, B., Raymond, N., Mercier, O., Mussot, S., Cohen-Kaminsky, S., et al. (2012). Pulmonary lymphoid neogenesis in idiopathic pulmonary arterial hypertension. Am. J. Respir. Crit. Care Med. *185*, 311–321.

Presta, M., Dell'Era, P., Mitola, S., Moroni, E., Ronca, R., and Rusnati, M. (2005). Fibroblast growth factor/fibroblast growth factor receptor system in angiogenesis. Cytokine Growth Factor Rev. *16*, 159–178.

Revest, J.M., Suniara, R.K., Kerr, K., Owen, J.J., and Dickson, C. (2001). Development of the thymus requires signaling through the fibroblast growth factor receptor R2-IIIb. J. Immunol. *167*, 1954–1961.

Shigematsu, S., Yamauchi, K., Nakajima, K., Iijima, S., Aizawa, T., and Hashizume, K. (1999). IGF-1 regulates migration and angiogenesis of human endothelial cells. Endocr. J. *46* (*Suppl*), S59–S62.

Sitnik, K.M., Kotarsky, K., White, A.J., Jenkinson, W.E., Anderson, G., and Agace, W.W. (2012). Mesenchymal cells regulate retinoic acid receptor-dependent cortical thymic epithelial cell homeostasis. J. Immunol. *188*, 4801–4809.

Srinivas, S., Watanabe, T., Lin, C.S., William, C.M., Tanabe, Y., Jessell, T.M., and Costantini, F. (2001). Cre reporter strains produced by targeted insertion of EYFP and ECFP into the ROSA26 locus. BMC Dev. Biol. *1*, 4.

Wang, X., Cho, B., Suzuki, K., Xu, Y., Green, J.A., An, J., and Cyster, J.G. (2011). Follicular dendritic cells help establish follicle identity and promote B cell retention in germinal centers. J. Exp. Med. *208*, 2497–2510.

White, A., Carragher, D., Parnell, S., Msaki, A., Perkins, N., Lane, P., Jenkinson, E., Anderson, G., and Caamaño, J.H. (2007). Lymphotoxin a-dependent and -independent signals regulate stromal organizer cell homeostasis during lymph node organogenesis. Blood *110*, 1950–1959.

White, A., Jenkinson, E., and Anderson, G. (2008). Reaggregate thymus cultures. J. Vis. Exp. *18*, 905.

Wong, K., Lister, N.L., Barsanti, M., Lim, J.M., Hammett, M.V., Khong, D.M., Siatskas, C., Gray, D.H., Boyd, R.L., and Chidgey, A.P. (2014). Multilineage potential and self-renewal define an epithelial progenitor cell population in the adult thymus. Cell Rep. *8*, 1198–1209.

Yi, T., Wang, X., Kelly, L.M., An, J., Xu, Y., Sailer, A.W., Gustafsson, J.A., Russell, D.W., and Cyster, J.G. (2012). Oxysterol gradient generation by lymphoid stromal cells guides activated B cell movement during humoral responses. Immunity *37*, 535–548.

Zachariah, M.A., and Cyster, J.G. (2010). Neural crest-derived pericytes promote egress of mature thymocytes at the corticomedullary junction. Science *328*, 1129–1135.

Zhang, C., Lu, L., Li, Y., Wang, X., Zhou, J., Liu, Y., Fu, P., Gallicchio, M.A., Bach, L.A., and Duan, C. (2012). IGF binding protein-6 expression in vascular endothelial cells is induced by hypoxia and plays a negative role in tumor angiogenesis. Int. J. Cancer *130*, 2003–2012.

Zuklys, S., Mayer, C.E., Zhanybekova, S., Stefanski, H.E., Nusspaumer, G., Gill, J., Barthlott, T., Chappaz, S., Nitta, T., Dooley, J., et al. (2012). MicroRNAs control the maintenance of thymic epithelia and their competence for T lineage commitment and thymocyte selection. J. Immunol. *189*, 3894–3904.